

# Flux Crystal Growth, Crystal Structure, and Optical Properties of New Germanate Garnet Ce<sub>2</sub>CaMg<sub>2</sub>Ge<sub>3</sub>O<sub>12</sub>

3

1

2

- Jie Chen<sup>1,2</sup>, Hong Yan<sup>1,2</sup>, Akihide Kuwabara<sup>3</sup>, Mark D. Smith<sup>4</sup>, Yuki Iwasa<sup>5</sup>, Hiraku Ogino<sup>5</sup>, 4
- 5 Yoshitaka Matsushita<sup>6</sup>, Yoshihiro Tsujimoto<sup>1,2,4\*</sup>, Kazunari Yamaura<sup>1,2</sup>, Hans-Conrad zur
- 6 Love4\*
- 7 <sup>1</sup>Research Center for Functional Materials, National Institute for Materials Science, Tsukuba, Japan
- 8 <sup>2</sup> Graduate School of Chemical Sciences and Engineering, Hokkaido University, Sapporo, Japan
- 9 <sup>3</sup> Nanostructures Research Laboratory, Japan Fine Ceramic Center, Atsuta, Japan
- 10 <sup>4</sup> Department of Chemistry and Biochemistry, University of South Carolina, Columbia, South
- Carolina, USA 11
- 12 <sup>5</sup> National Institute of Advance Industrial Science and Technology, Tsukuba, Japan
- 13 <sup>6</sup> Materials Analysis Station, National Institute for Materials Science, Tsukuba, Japan

- 15 \* Correspondence:
- Dr. Yoshihiro Tsujimoto 16
- TSUJIMOTO. Yoshihiro@nims.go.jp 17
- 18 Prof. Hans-Conrad zur Loye
- 19 ZURLOYE@mailbox.sc.edu
- 20 Prof. Hans-Conrad zur Loye
- 21 ZURLOYE@mailbox.sc.edu
- 22 Keywords: flux crystal growth<sub>1</sub>, garnet<sub>2</sub>, germanate<sub>3</sub>, single crystal<sub>4</sub>, photoluminesence<sub>5</sub>.
- 23 Abstract
- 24 A new germanate garnet compound, Ce<sub>2</sub>CaMg<sub>2</sub>Ge<sub>3</sub>O<sub>12</sub>, was synthesized via flux crystal growth.
- 25 Truncated spherical, reddish-orange single crystals with a typical size of 0.1–0.3 mm were grown out
- of a BaCl<sub>2</sub>–CaCl<sub>2</sub> melt. The single crystals were characterized by single-crystal X-ray diffraction 26
- 27 analysis, which revealed that it adopted a cubic garnet-type structure with a = 12.5487(3) Å in the
- 28 space group Ia-3d. Its composition is best described as  $A_3B_2C_3O_{12}$ , where Ce/Ca, Mg, and Ge occupied
- 29 the A, B, and C sites, respectively. A UV-vis-NIR absorption spectroscopy measurement on the
- 30 germanate garnet revealed a clear absorption edge corresponding to a band gap of 2.21 eV ( $\lambda = 561$
- nm). First-principle calculations indicated that the valence band maximum was composed of Ce 4f 31
- 32 bands, whereas the conduction band minimum mainly consisted of Ce 5d bands. These findings explain
- 33 the observed absorption edge through the Ce  $4f \rightarrow 5d$  absorption. Photoluminescence emission spectra
- 34 exhibited a very broad peak centered at 600 nm, corresponding to transition from the lowest energy d
- 35 level to the 4*f* levels.

#### 1 Introduction

36

57

58

59

60

61

62

63

64

65

66

37 The garnet structure, having the general chemical formula  $\{A\}_3[B]_2(C)_3O_{12}$ , has been widely studied 38 as a host material for various optical applications, such as laser amplifiers, color converters, 39 scintillators, and cathode ray phosphors [1]. In particular, the Ce<sup>3+</sup>-doped Y<sub>3</sub>Al<sub>5</sub>O<sub>12</sub> garnet phosphor 40 (YAG:Ce) is one of the most interesting materials in terms of practical application as a blue-to-yellow 41 converter in white-emitting diodes. Although YAG:Ce exhibits good thermal and chemical stability and high luminescence efficiency, improvements to the low thermal quenching temperature and cool 42 43 correlated color temperature remain significant issues [2] [3] [4]. In principle, the 5d-4f emission bands 44 in Ce<sup>3+</sup>-doped phosphors are strongly influenced by the host lattice through crystal field splitting of the 5d levels of the  $Ce^{3+}$  ion. In the garnet host, there are three types of cation sites: the  $\{A\}$  site with 8-45 46 fold dodecahedral coordination, the [B] site with 6-fold octahedral coordination, and the (C) site with 47 4-fold tetrahedral coordination (Figure 1). The A site is typically occupied by rare-earth (RE) ions such as  $La^{3+}$ ,  $Gd^{3+}$ , or  $Lu^{3+}$ , as well as by  $Y^{3+}$ , and by alkaline earth ions such as  $Ca^{2+}$ . The B site is occupied 48 by smaller ions that prefer octahedral coordination environments, such as Mg<sup>2+</sup> Mn<sup>3+</sup>, Fe<sup>3+</sup>, Sc<sup>3+</sup>, Al<sup>3+</sup>, 49 or  $Zr^{4+}$ , while the C site accommodates ions that take on tetrahedral coordination, including  $Al^{3+}$ ,  $Ga^{3+}$ , 50 Si<sup>4+</sup>, or Ge<sup>4+</sup> ions. The dodecahedral site, which the trivalent Ce<sup>3+</sup> ion prefers to occupy, connects to 51 the adjacent A, B, and C sites through common oxygen atoms via corner and edge sharing. Thus, the 52 53 crystal field impinging on the  $Ce^{3+}$  ions is created not only by the A site cations but also the B and C 54 site cations [5, 6] [7]. Owing to the wide range of cations that can be accommodated by the garnet 55 structure, new compositions of garnet phosphors that compensate for the above-mentioned 56 shortcomings of YAG:Ce have been successfully synthesized.

When considering the crystal chemistry of the garnet family, the ability of the cation sites, especially the *A* site, to accommodate different elements, is an important factor [8]. A large number of garnet compounds have been previously reported [1, 9-11] but the variety of *RE* ions in the *A* site is typically limited to *RE* = Gd–Lu and Y, all smaller than the desirable Eu<sup>3+</sup> cation, because incorporation of larger cation causes markedly unfavorable lattice distortions around the dodecahedral sites. To the best of our knowledge, only very few garnet compositions that include early *RE* ions larger than Gd<sup>3+</sup> have been synthesized (via various techniques such as the sol-gel method and hydrothermal reaction), and include: Eu<sub>3</sub>Al<sub>5</sub>O<sub>12</sub> [12], *RE*<sub>3</sub>Te<sub>2</sub>Li<sub>3</sub>O<sub>12</sub> (*RE* = Pr–Eu) [13], *RE*<sub>3</sub>W<sub>2</sub>Li<sub>3</sub>O<sub>12</sub> (*RE* = Pr, Nd) [13] (Kasper, 1969), *RE*<sub>3</sub>Fe<sub>5</sub>O<sub>12</sub> (*RE* = Pr–Eu) [14] [15] [16] [17], La<sub>3</sub>Sc<sub>2</sub>Ga<sub>3</sub>O<sub>12</sub> [18], *RE*<sub>3</sub>Ga<sub>5</sub>O<sub>12</sub> (*RE* = Pr–Eu) [19] [20], Li<sub>7</sub>La<sub>3</sub>Zr<sub>2</sub>O<sub>12</sub> [21], and Li<sub>5</sub>La<sub>3</sub>Sb<sub>2</sub>O<sub>12</sub> [22]. It is notable that even among these, achieving a garnet

- composition with  $Ce^{3+}$  fully occupying the A site is challenging; however,  $Ce^{3+}$  doping as high as 56
- at.% with respect to Y<sup>3+</sup> has been achieved in YFe<sub>5</sub>O<sub>12</sub> via the glycothermal process.[23]
- 69 In this study, we report the flux crystal growth of the new metastable germanate oxide
- $\{\text{Ce}_2\text{Ca}\}[\text{Mg}]_2(\text{Ge})_3\text{O}_{12},$  which crystalizes in the garnet structure in the space group Ia-3d with a=
- 71 12.5487(3) Å. The garnet phase was synthesized via the flux crystal growth method where truncated
- spherical, reddish-orange single crystals were obtained from a BaCl<sub>2</sub>–CaCl<sub>2</sub> melt. High-temperature
- solid state reactions failed to yield the target phase, even as a polycrystalline powder, suggesting that
- 74 the phase is metastable. Herein we discuss the crystal structure, electronic structure, and optical
- properties of Ce<sub>2</sub>CaMg<sub>2</sub>Ge<sub>3</sub>O<sub>12</sub>.

## 2 Experimental

76

77

90

## 2.1 Crystal Growth

- Single crystals of Ce<sub>2</sub>CaMg<sub>2</sub>Ge<sub>3</sub>O<sub>12</sub> were grown via the flux method using a eutectic BaCl<sub>2</sub>–CaCl<sub>2</sub>
- mixture[24]. For Ce<sub>2</sub>CaMg<sub>2</sub>Ge<sub>3</sub>O<sub>12</sub>, a magnesia crucible was loaded with 1 mmol CeO<sub>2</sub> (Aldrich, 4N),
- 1 mmol of GeO<sub>2</sub> (Rare Metallic, 4N), 1 mmol of S (High Purity Materials, 4N), 3.1 mmol of BaCl<sub>2</sub>
- 81 (Rare Metallic, 3N), and 3.1 mmol of CaCl<sub>2</sub> (Rare Metallic, 3N). The top of the tube was closed with
- 82 a magnesia cap, and the tube was sealed inside a silica tube under vacuum. As described later, the
- 83 magnesia tube was found to act as a magnesium source. The starting materials were heated in a box
- 84 furnace to 900 °C at 150 °C/h, held for 25 h, cooled to 500 °C at 5 °C/h, and then allowed to cool
- 85 naturally to room temperature. The products were washed in distilled water, aided by sonication, before
- 86 the reddish-orange transparent truncated spherical crystals of Ce<sub>2</sub>CaMg<sub>2</sub>Ge<sub>3</sub>O<sub>12</sub>, together with
- 87 colorless transparent crystals of CeOCl, were collected via vacuum filtration. The typical dimensions
- of the single crystals of the garnet compound were  $0.3 \times 0.3 \times 0.3 \text{ mm}^3$  (Figure 2). The structure of
- 89 Ce<sub>2</sub>CaMg<sub>2</sub>Ge<sub>3</sub>O<sub>12</sub> was determined by single-crystal X-ray diffraction.

### 2.2 Single crystal structure determination

- 91 X-ray intensity data from an orange polyhedron were collected at 301(2) K using a Bruker D8 QUEST
- 92 diffractometer equipped with a PHOTON 100 CMOS area detector and an Incoatec microfocus source
- 93 (Mo K $\alpha$  radiation,  $\lambda = 0.71073$  Å) [25]. The data collection covered 100% of the reciprocal space to
- $2\theta_{\text{max}} = 75.2^{\circ}$ , with an average reflection redundancy of 35.3 and  $R_{\text{int}} = 0.064$  after absorption
- orrection. The raw area detector data frames were reduced and corrected for absorption effects using

- 96 the SAINT+ and SADABS programs [26] [25]. Final unit cell parameters were determined by least-
- 97 squares refinement of 3812 reflections taken from the data set. An initial structural model was obtained
- 98 with SHELXT [27]. Subsequent difference Fourier calculations and full-matrix least-squares
- refinement against  $F^2$  were performed with SHELXL-2018 using the ShelXle interface [28].

## 100 2.3 Solid state synthesis

105

106

107

108

109

110

111

112

113

114

115

116

117

118

119

120

121

122

123

- The synthesis of polycrystalline powder samples of Ce<sub>2</sub>CaMg<sub>2</sub>Ge<sub>3</sub>O<sub>12</sub> was attempted using CeO<sub>2</sub>,
- 102 CaCO<sub>3</sub> (or CaO), MgO, and GeO<sub>2</sub> in a stoichiometric ratio. The mixture was ground intimately,
- pelletized, and heated in a flowing  $N_2$  or  $H_2$  (20%)—Ar (80%) mixed gas atmosphere or in an evacuated
- sealed tube using a tubular furnace at temperatures ranging from 900 to 1500 °C.

#### 2.4 XRD, UV-vis, PL, EPL, and magnetic measurements

Single crystals of Ce<sub>2</sub>CaMg<sub>2</sub>Ge<sub>3</sub>O<sub>12</sub> were crushed with an agate mortar and pestle to obtain fine powders used for obtaining synchrotron X-ray powder diffraction (SXRD) patterns, UV-vis diffuse reflectance spectra, and photoluminescence (PL) and photoluminescence excitation (PLE) spectra. The products obtained via solid state reactions were examined at room temperature by powder XRD analysis using a Rigaku MiniFlex X-ray diffractometer (Cu  $K\alpha$  radiation) in the  $2\theta$  range of 5–65° with a step size of 0.04°. SXRD measurement was performed at room temperature using a one-dimensional detector installed on BL15XU, NIMS beamline at SPring-8 in Japan. The synchrotron radiation X-rays were monochromatized to a wavelength of 0.65298 Å. The Ce<sub>2</sub>CaMg<sub>2</sub>Ge<sub>3</sub>O<sub>12</sub> powder sample was loaded into a 0.1-mm diameter glass capillary. The diffraction data were recorded in 0.003° increments over the range 2-60° and analyzed by Rietveld refinement using the program RIETAN-FP [29]. Diffuse reflectivity measurements were performed at room temperature using a Shimadzu UV-2600 spectrophotometer equipped with an ISR-2600Plus integration sphere. The diffuse reflectance data were internally converted to absorbance by the instrument using the Kubelka–Munk function. The PLE and emission spectra were recorded using a fluorescence spectrophotometer (Hitachi F-7000). The magnetic susceptibility of Ce<sub>2</sub>CaMg<sub>2</sub>Ge<sub>3</sub>O<sub>12</sub> was measured using a SQUID magnetometer (Quantum Design, MPMS-XL). The crushed single crystals were measured at an applied magnetic field (H) of 1 kOe in the range of 10–300 K under both zero-field-cooled (ZFC) and field-cooled (FC) conditions.

#### 2.5 First-principles calculations

First-principles total energy calculations of Ce<sub>2</sub>CaMg<sub>2</sub>Ge<sub>3</sub>O<sub>12</sub> were performed using the projector 124 125 augmented wave method[30][31] as implemented in the Vienna Ab-initio Simulation Package (VASP) [32] [33] [34]. In the present study, the cut-off energy for the plane wave basis was 550 eV. The 126 127 exchange-correlation interaction potentials of electrons were handled within a framework of the 128 generalized gradient approximation (GGA) of with the PBEsol type[35]. The configurations of the valence electrons of Ce, Ca, Mg, Ge and O were  $5s^2 5p^6 4f^1 5d^1 6s^2$ ,  $3s^2 3p^6 4s^2$ ,  $2p^6 3s^2$ ,  $3d^{10} 4s^2 4p^2$ 129 and  $2s^2 2p^4$ , respectively. Spin-polarized calculations were carried out. For Ce ions, the effect of the 130 strong correlation interaction of the 4f orbital was treated based on the GGA+U method. [36] The value 131 132 of U was set to be 5.4 eV in this study. [37] [38] Structure optimization calculations were carried out 133 until the residual forces were less than 0.02 eV/Å.

#### 3 Results and Discussion

134

135

136

137

138

139

140

141

142

143

144

145

146

147

148

149

150

151

152

153

154

#### 3.1 Crystal growth and structure determination

After washing the products inside the magnesia tube with water to remove the solidified flux, we found that reddish-orange single crystals had grown on the inner wall of the tube (Figure 2) alongside with a plate-like pale-purple crystalline CeOCl byproduct. The EDS analysis of the reddish-orange crystals revealed the presence of Ce, Ca, Mg, and Ge in approximate atomic ratios of 1.9:1.0:2.1:2.6. The origin of the magnesium is the magnesia tube that, apparently, was slightly dissolved by the flux during the reaction. Single-crystal X-ray diffraction analysis revealed that the product crystallized in the cubic system with a = 12.5479(4) Å. The space group Ia-3d (space group no. 230) was uniquely determined by the pattern of systematic absences in the intensity data and confirmed by structure solution. The product exhibits a garnet-type structure, wherein the asymmetric unit consists of one mixed Ce/Ca atomic site (Ce1/Ca1, site 24c), one Ge site (Ge1, 24d), one Mg site (Mg1, 16a,), and one O site (O1, 96h). The composition of site 24c was determined by trial refinements of several models incorporating cationic elements determined by EDS to be present in the crystals (i.e., only Ce, Ca, Mg, and Ge). Modeling the site with mixed Ce/Ca occupancy resulted in the most reasonable model and is consistent with their similar ionic radii ( $r_{Ce}^{3+} = 1.143 \text{ Å}$ ,  $r_{Ca}^{2+} = 0.97 \text{ Å}$ ) [39] and their observed bond distances to O (2.427(4) and 2.547(4) Å, respectively). To maintain overall charge balance, the Ce and Ca occupancies were fixed at 2/3 Ce and 1/3 Ca. Trial refinements with Ce and Ca occupancies constrained to sum to 1.0 but otherwise free to vary, refined closely to these values, supporting the decision to fix the occupancies at 2/3 Ce and 1/3 Ca. All atoms were refined with anisotropic displacement parameters. The final refined chemical composition was Ce<sub>2</sub>CaMg<sub>2</sub>Ge<sub>3</sub>O<sub>12</sub>,

155 which is consistent with the result of the EDS analysis. The  $R_{int}$  and  $wR_2$  converged to reasonable 156 values of 3.83 and 5.51%, respectively. The goodness-of-fit value was 1.29. The incorporation of Ce(III) ions into the structure was consistent with the reddish-orange sample color. Details of the 157 158 structure refinement are listed in Table 1. Atomic coordinates and atomic displacement parameters 159 are listed in Tables 2 and S1, respectively. Selected bond distances and bond angles are compiled in 160 Table 3. 161 Figure 3 shows the room-temperature synchrotron X-ray diffraction pattern collected from a powder 162 sample obtained by grinding hand-picked single crystals. The model determined by the SCXRD 163 analysis was used for the Rietveld refinement. The calculated pattern well reproduced the observed 164 pattern as the fitting converged smoothly with reasonable reliability factors,  $R_{wp} = 5.37$ ,  $R_B = 3.45$ , and  $R_{\rm F} = 2.92$ . The final refined crystallographic data, including the atomic coordinates and isotropic 165 166 displacement parameters are listed in Table S2. The results are consistent with the results obtained 167 from the SCXRD analysis. 168 3.2 **Solid state reaction** 169 Synthesis of a polycrystalline sample of Ce<sub>2</sub>CaMg<sub>2</sub>Ge<sub>3</sub>O<sub>12</sub> was attempted by solid-state reactions 170 using a stoichiometric mixture of CeO<sub>2</sub>, CaCO<sub>3</sub> (or CaO), MgO, and GeO<sub>2</sub>. The reactions were 171 carried out under vacuum, with mixed H<sub>2</sub>(20%)-Ar(80%) gas or N<sub>2</sub> gas atmospheres at temperatures 172 between 900 and 1300 °C. Unfortunately, none of the reaction conditions we examined yielded the 173 target phase; but a substantial amount of unreacted CeO<sub>2</sub> always remained in the products (see Figure 174 S1). A garnet structure was obtained as a minor phase at 1300 °C in the N<sub>2</sub> gas atmosphere; however, 175 the lattice parameter of the garnet phase was smaller by 0.5% compared with that for 176 Ce<sub>2</sub>CaMg<sub>2</sub>Ge<sub>3</sub>O<sub>12</sub> and the product was dark grayish-green. Therefore, if Ce atoms were incorporated 177 into the lattice, the garnet phase obtained by solid state reaction should have a lower Ce concentration 178

#### 3.3 Stability of the garnet structure

179

180

181

- 182 As described earlier, the garnet structure can accommodate a wide range of elements in the three
- 183 different cation sites, but the underlying stability of the garnet structure, including its tolerance for

than that of Ce<sub>2</sub>CaMg<sub>2</sub>Ge<sub>3</sub>O<sub>12</sub>. Further heating at the same temperature after regrinding and

CeO<sub>2</sub>, suggesting that the garnet phase was metastable under these reaction conditions.

pelletizing resulted in a partial decomposition of the garnet phase and an increase in the amount of

184 RE ions, is not yet well understood. Our present germanate garnet exhibited an unusual occupancy of

- two-thirds of the *A* sites by  $Ce^{3+}$  ions, a  $Ce^{3+}$  concentration substantially higher than the 56 at.%  $Ce^{3+}$ -doping concentration found in  $Y_{1-x}Ce_xFe_5O_{12}$  (x = 1.7).[23] Very recently, Song *et al.* have
- formulated the tolerance factor ( $\tau$ ) of the garnet structure,[40] which is analogous to the Goldschmidt
- tolerance factor describing the relationship of the chemical compositions and structural stability in
- perovskites. [41] The  $\tau$  of the garnet structure is expressed as

190 
$$\tau = \frac{3\sqrt{(r_B + r_0)^2 + \frac{4}{9}(r_A + r_0)^2}}{2(r_C + r_0)}$$
 (Eq. 1)

- where  $r_A$ ,  $r_B$ ,  $r_C$ , and  $r_O$  represent the ionic radii of the A, B, C site cations and  $O^{2-}$  ion, respectively.
- The tolerance factor calculated for more than 100 garnet compounds falls within the range of 0.75 to
- 193 1.33. For the formula  $RE_3B_2C_3O_{12}$ . (RE = La-Lu, Y; B = C = Fe, Al, Ga), the  $\tau$  values systematically
- increase toward unity with decreasing size of the RE ions, e.g., 0.76 to 0.93 from La to Lu for
- RE<sub>3</sub>Al<sub>5</sub>O<sub>12</sub> and 0.89 to 1.02 for  $RE_3$ Fe<sub>5</sub>O<sub>12</sub>). [40] This is consistent with the general trend observed
- for their structural stability when containing RE ions. The formula  $RE_2$ CaMg<sub>2</sub>Ge<sub>3</sub>O<sub>12</sub> (RE = La-Lu,
- 197 Y), including hypothetical compositions, exhibits a similar size dependence of the tolerance factor,
- but the τ values range from 1.06 for La, through 1.07 for Ce, to 1.15 for Lu. The stabilization of
- 199 Ce<sub>2</sub>CaMg<sub>2</sub>Ge<sub>3</sub>O<sub>12</sub> with a τ value close to unity seems to be compatible with the geometric
- 200 requirements for the garnet structure. However, a favorable tolerance factor does not assure the
- success of the target phase formation via chemical synthesis. In fact, the solid-state reactions we
- examined to obtain Ce<sub>2</sub>CaMg<sub>2</sub>Ge<sub>3</sub>O<sub>12</sub> were not successful. At present, the reason for the large
- amount of Ce ions incorporated into the garnet lattice is unclear; however, it is likely that the molten
- salts used in this study play a crucial role in stabilizing the phase under the flux reaction conditions.
- 205 From the PXRD data of the products obtained by solid state reactions, it is apparent that CeO<sub>2</sub> was
- 206 not fully consumed in the reactions, indicating its low reactivity and slow atomic diffusion even at
- high temperatures. In the flux reaction, the BaCl<sub>2</sub>–CaCl<sub>2</sub> salt likely dissolves CeO<sub>2</sub> powder at a
- 208 relatively low temperature, where the fact that the starting materials are now in solution is expected
- 209 to decrease considerably the activation energy for reaction between the starting materials and thus
- 210 yield the target garnet phase. We surmise that the Ca-Cl melt at high temperatures under vacuum acts
- as a reducing agent for Ce ions, likely forming Cl<sub>2</sub>. The formation of Ce<sup>3+</sup> in the halide melt favors
- the stabilization of Ce<sub>2</sub>CaMg<sub>2</sub>Ge<sub>3</sub>O<sub>12</sub> as well as of the byproduct CeOCl. Sulfur, which was a starting
- 213 material for the flux reaction, was not found to significantly contribute to either the reduction of Ce

214 ions nor to the formation of Ce<sub>2</sub>CaMg<sub>2</sub>Ge<sub>3</sub>O<sub>12</sub>. Performing the flux crystal growth in the absence of 215 sulfur results in the same mixed product formation. 216 3.4 Optical and magnetic properties 217 Figure 4(a) shows the UV-vis absorption spectrum collected for Ce<sub>2</sub>CaMg<sub>2</sub>Ge<sub>3</sub>O<sub>12</sub>, exhibiting a clear 218 absorption edge at around 560 nm. An extrapolation of the linear portion of the absorption curve to 219 the x-axis indicates an optical band gap of  $E_g = 2.22$  eV. This steep increase in the absorption is 220 followed by two broad sub-bands centered at 458 and 305 nm, also observed in the UV-vis 221 absorption curves of YAG:Ce. These two absorption peaks can be assigned to the optical transitions from the Ce 4f ground state to the lowest and second-lowest excited states of the Ce 5d orbitals ( $5d_1$ 222 223 and  $5d_2$ , respectively). [2] A third weak peak at around 250 nm is probably due to defects or 224 impurities. The lowest absorption is in the blue spectral region, which results in the reddish orange 225 color of the garnet compound. The photoluminescence emission (PE) and excitation (PLE) spectra of 226 Ce<sub>2</sub>CaMg<sub>2</sub>Ge<sub>3</sub>O<sub>12</sub> are shown in Figure 4(b). The PE spectrum excited at 519 nm contains a broad 227 band centered around 600 nm, which could be assigned to the transition from the  $5d_1$  level to the two 228 4f levels split by spin-orbit coupling into  ${}^{2}F_{5/2}$  and  ${}^{2}F_{7/2}$ . The maximum value of the emission band for 229 Ce<sub>2</sub>CaMg<sub>2</sub>Ge<sub>3</sub>O<sub>12</sub> is red-shifted compared to that of Y<sub>2</sub>Mg<sub>3</sub>Ge<sub>3</sub>O<sub>12</sub>:Ce(2%) [42] but comparable to 230 that for Gd<sub>2</sub>Mg<sub>3</sub>Ge<sub>3</sub>O<sub>12</sub>:Ce(2%) [43]. 231 Figure 5 shows the temperature evolution of the magnetic susceptibility  $\chi$  (= M/H) measured in a 232 magnetic field H = 1 kOe. Both the ZFC and FC data increase smoothly with decreasing temperature, 233 indicative of a paramagnetic state persisting down to low temperatures. No hysteresis was observed 234 in the temperature range between 10 and 300 K. Fitting  $\chi(T)$  to the Curie–Weiss law yields C =235 1.407(4) (emu K/mol) and  $\theta = -59.9(9)$  K, where C and  $\theta$  stand for the Curie and Weiss constants, 236 respectively. The C value is somewhat smaller than the theoretical value expected from two mol Ce<sup>3+</sup> ions with  ${}^2F_{5/2}$  per formula unit. The negative  $\theta$  value suggests that  $Ce^{3+}$  ions are 237 238 antiferromagnetically coupled to each other. The absence of a long-range magnetic order is probably 239 due to a random distribution of Ce and Ca atoms on the 24c site 240 3.5 Theoretical calculations 241 From the experimental crystal structure analysis of Ce<sub>2</sub>CaMg<sub>2</sub>Ge<sub>3</sub>O<sub>12</sub>, Ce and Ca ions are found to 242 occupy the A site of the  $A_3B_2C_3O_{12}$  garnet structure. In first principles calculations using structure

models under periodic boundary conditions, mixed occupancy of atomic sites cannot be directly

244 computed. Therefore, we initially determined the preferred distribution of Ce and Ca ions on the A 245 site with a ratio of 2:1 in a fixed size model having the garnet structure. We chose a primitive unit cell of the garnet structure as a base model. Structure models having symmetrically non-equivalent 246 247 configurations of Ce and Ca ions were constructed. In total, 20 independent configurations of Ce and 248 Ca ions on the A-site were found from the base model using the CLUPAN code. [44] The mesh size 249 of k-point sampling was  $3 \times 3 \times 3$  in the Brillouin zone of the input structure models. We compared 250 the total energies of these models obtained by structure optimization calculations. 251 From the series of total energy calculations of Ce<sub>2</sub>CaMg<sub>2</sub>Ge<sub>3</sub>O<sub>12</sub> models, the most stable configuration that was found is shown in Figure 6. We analyzed the electronic structures of this 252 model. Figure 7 shows total density of states (tDOS) and projected partial density of states (pDOS) of 253 each constituent element. In Figure 7, the energy level of a valence band top is set to be 0 eV on the 254 255 horizontal axes. Positive and negative values on the vertical axes indicate the DOS of up-spin and 256 down-spin, respectively. The tDOS values show that the calculated band gap is about 2.2 eV, which 257 is in a good agreement with the value estimated from the UV-vis absorption spectrum. It can be 258 clearly seen that very sharp spikes of the DOS exist at the topmost energy levels of the occupied 259 states. Such sharp DOS peaks indicate strong localization states of the electron orbitals. From the 260 pDOS values, we can see that these peaks originate from the occupied 4f orbital of the Ce<sup>3+</sup> ions. The 261 DOS near the conduction band bottom seems to be mainly composed of an unoccupied 5d orbital of Ce<sup>3+</sup> ions and a 4s orbital of the Ge<sup>4+</sup> ions. 262

#### 4 Conclusion

263

273

264 We have successfully synthesized a new metastable germanate garnet, Ce<sub>2</sub>CaMg<sub>2</sub>Ge<sub>3</sub>O<sub>12</sub>, using a 265 flux crystal growth method. Reddish-orange single crystals were grown in a reactive MgO tube; 266 however, the polycrystalline sample could not be prepared via a solid state reaction. Flux reactions 267 are clearly useful for extending the garnet family to compositions that include the early lanthanide 268 metals, especially those larger than Gd, which are been less explored. The PL intensity was so weak that it could not be confirmed visually; this is probably due to Ce<sup>3+</sup>-concentration quenching effects 269 or photoionization involving a charge transfer between Ce<sup>3+</sup> and Ge<sup>4+</sup>.[45, 46] Work to synthesize La 270 271 or RE (< Ce<sup>3+</sup>)-doped Ce<sub>2</sub>CaMg<sub>2</sub>Ge<sub>3</sub>O<sub>12</sub> and the substitution of Si for Ge, which would enhance PL 272 properties, is ongoing.

#### **5** Conflict of Interest

- The authors declare that the research was conducted in the absence of any commercial or financial
- 275 relationships that could be construed as a potential conflict of interest.

#### 276 **6 Author Contributions**

- 277 The manuscript was written through contributions of all authors. All authors have given approval to
- the final version of the manuscript.
- **279 7 Funding**
- 280 Research grants from JSPS KAKENHI (Grant no. 15H02024, 16H06438, 16H06441, 19H02594,
- 281 19H04711, 17H05493, 16H06439, 16K21724) and Innovative Science and Technology Initiative for
- Security, ATLA, Japan. Research Grant from UofSC (NSF grant DMR-1806279).
- 283 8 Acknowledgments
- We thank Dr. Y. Katsuya, Dr. M. Tanaka, and Prof. O. Sakata for their assistance in performing the
- 285 SXRD experiments at SPring-8 (Proposal no. 2018B4502, 2019A4501).
- 286 9 Reference
- 287 **10 Supplementary Material**
- 288 CIF files of Ce<sub>2</sub>CaMg<sub>2</sub>Ge<sub>3</sub>O<sub>10</sub> based on single crystal XRD data. Anisotropic displacement parameters
- for Ce<sub>2</sub>CaMg<sub>2</sub>Ge<sub>3</sub>O<sub>10</sub>. Crystallographic data obtained from the Rietveld refinement against the SXRD
- 290 data. Powder XRD data collected from the products of the solid state reactions.

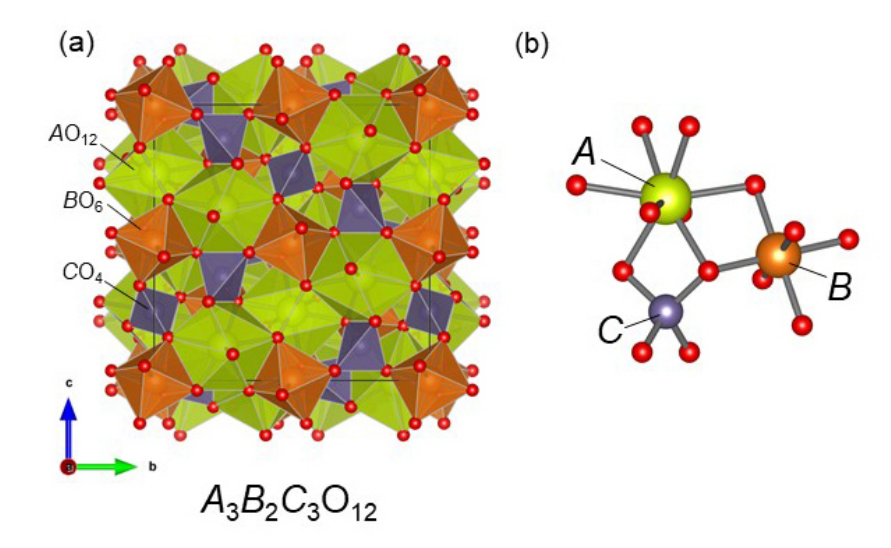


Figure 1. (a) Crystal structure of the garnet compound  $A_3B_2C_3O_{12}$  and (b) the local coordination environment around the metal cations. In Ce<sub>2</sub>CaMg<sub>2</sub>Ge<sub>3</sub>O<sub>12</sub>, Ce/Ca, Mg, and Ge atoms occupy the A, B, and C sites, respectively.

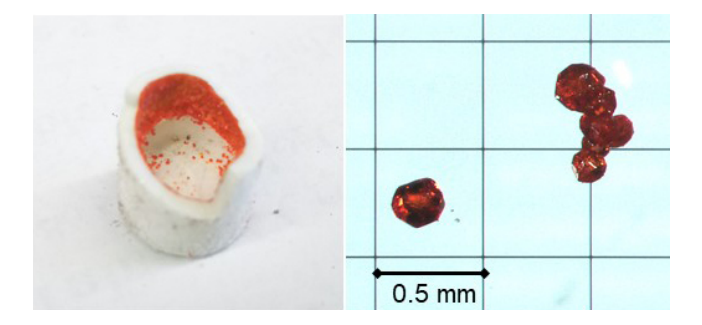


Figure 2. Photographs of single crystals of  $Ce_2CaMg_2Ge_3O_{12}$  grown on the inner wall of a MgO crucible.

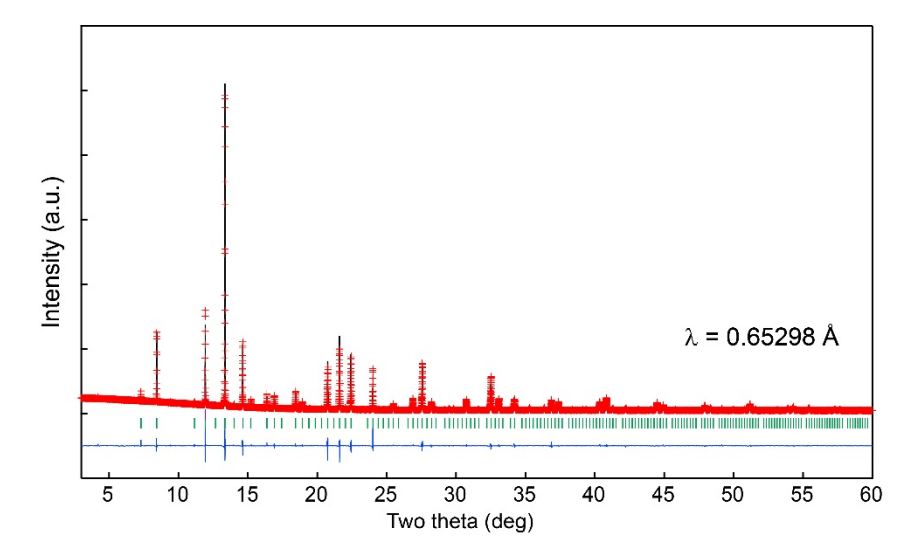


Figure 3. Observed (crosses), calculated (upper solid line), and difference (lower solid line) plots obtained from the Rietveld analysis of the room temperature synchrotron X-ray powder diffraction data collected using ground single crystals of Ce<sub>2</sub>CaMg<sub>2</sub>Ge<sub>3</sub>O<sub>12</sub>. Vertical lines represent expected Bragg peak positions.

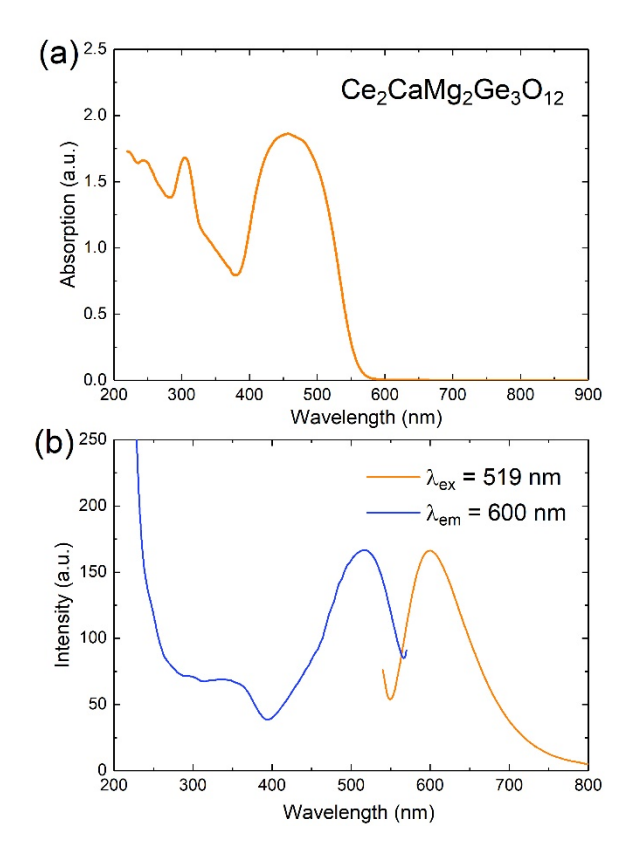


Figure 4. (a) UV–vis absorption spectrum, and (b) photoluminescence emission ( $\lambda_{ex} = 519$  nm) and excitation ( $\lambda_{em} = 600$  nm) spectra for Ce<sub>2</sub>CaMg<sub>2</sub>Ge<sub>3</sub>O<sub>12</sub>, collected at room temperature.

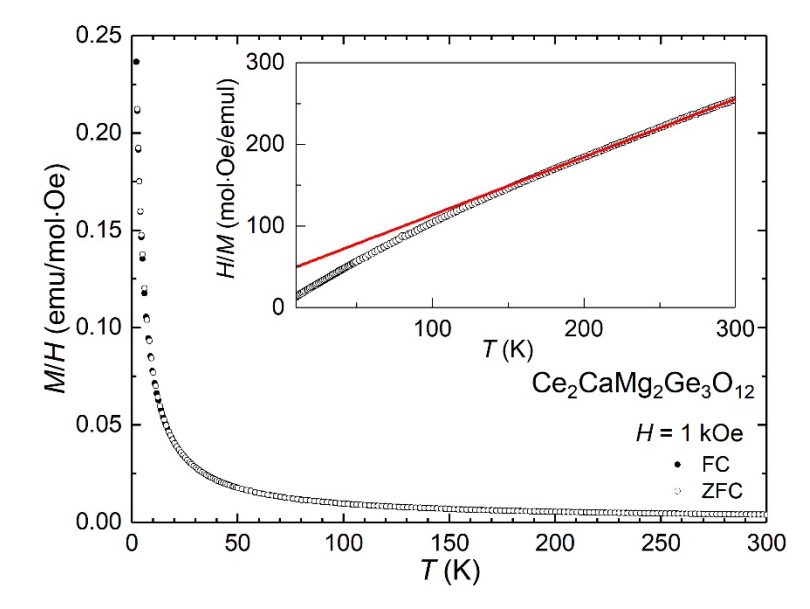


Figure 5. Magnetic susceptibility of  $Ce_2CaMg_2Ge_3O_{12}$ , measured in a magnetic field of 1 kOe. The inset shows its inverse  $\chi$  vs T plot. The red solid line is the fit to the Curie-Weiss law.

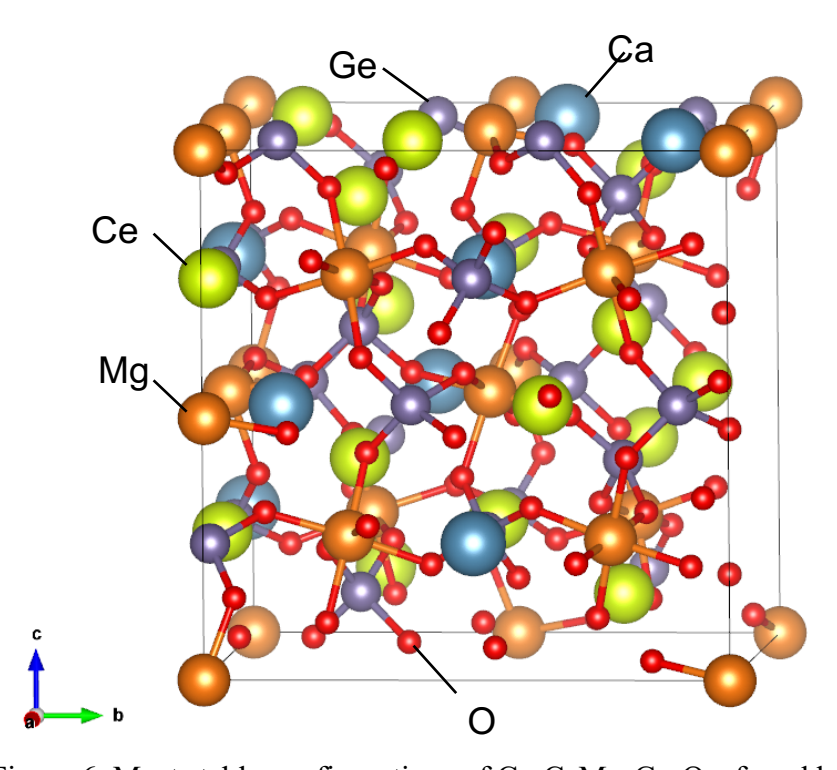


Figure 6. Most stable configurations of Ce<sub>2</sub>CaMg<sub>2</sub>Ge<sub>3</sub>O<sub>12</sub> found by a series of first principles calculations in the present study. Search conditions are described in the main text.

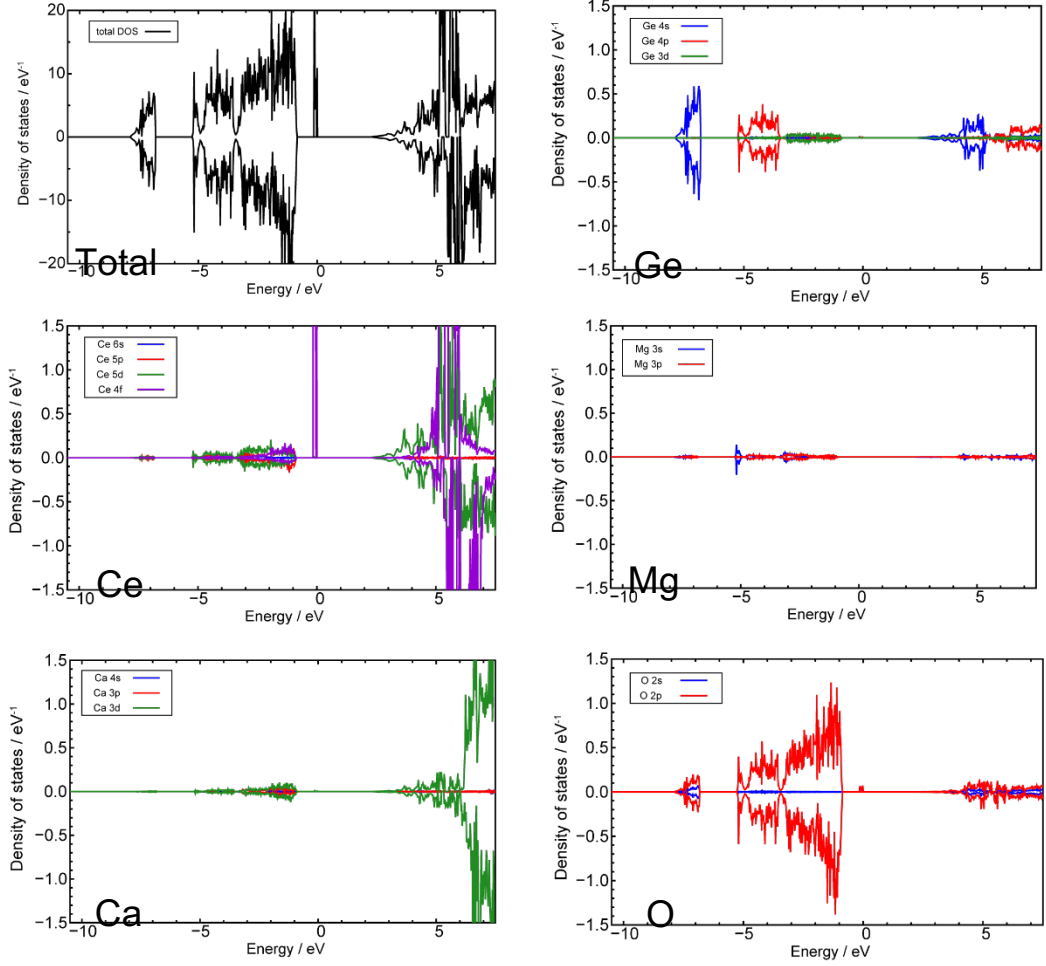


Figure 7. Total and projected partial density of states calculated from the model shown in Fig.6. The energy level of a valence band top is set to be 0 eV on the horizontal axes. Positive and negative values of the vertical axes indicate the DOS of up-spin and down-spin, respectively. Blue, red, green, and purple lines indicate the s, p, d, and f orbitals of each element, respectively.

Table 1. Results of structural refinement of  $Ce_2CaMg_2Ge_3O_{12}$  using single-crystal XRD data

Space group	Ia-3d	
Crystal system	Cubic	
a (Å)	12.5487(3)	
$V(Å^3)$	1976.04(14)	
Z	8	
Density (g/cm <sup>3</sup> )	5.235	
Temperature (K)	301(2)	
θ range (°)	3.978–37.590	
$\mu$ (mm <sup>-1</sup> )	18.765	
Crystal dimensions (mm <sup>3</sup> )	0.080×0.050×0.030	
Collected reflections	17162	
Unique reflections	445	
$R_{ m int}$	0.0645	
GOF	1.286	
$R_1(F)$ for $Fo^2 > 2\sigma(Fo^2)$	0.0383	
$R_{\rm w}(Fo^2)$	0.0551	
$\Delta  ho_{ m max}/\Delta  ho_{ m min} \ ({ m e}/{ m \AA}^3)$	0.931/-1.069	

Table 2. Atomic coordinates and equivalent isotropic displacement parameters  $U_{\rm eq}$  for  $Ce_2CaMg_2Ge_3O_{12}$  obtained from the structure refinement using single-crystal XRD data

Atom	Site	x	y	Z	$g^a$	$U_{\text{eq}}$ (Å <sup>2</sup> ×10 <sup>2</sup> )
Ce1	24c	1/8	0	1/4	0.667	0.737(15)
Cal	24c	1/8	0	1/4	0.333	0.737
Mg1	16a	0	0	0	1	0.75(5)
Ge1	24d	3/8	0	1/4	1	0.0660(18)
O1	96h	0.0948(2)	0.1976(3)	0.2852(3)	1	0.68(5)

328 <sup>a</sup> g represents site occupancy.

Table 3. Selected interatomic distances and bond angles of  $Ce_2CaMg_2Ge_3O_{12}$  at 301 K

	Bond distance (Å)		Bond angle (deg)
Ce/Ca-O×4	2.427(4)	Ce/Ca-O-Mg	97.48(12)
Ce/Ca –O×4	2.547(4)	Ce/Ca-O-Mg	101.26(15)
Mg-O×6	2.102(3)	Ce/Ca –O–Ge×2	95.60(13)
Ge-O×4	1.766(3)	Ce/Ca-O-Ce/Ca×2	101.13(14)

330

329

331

332

333

334

**Uncategorized References** 

- 335 1. Xia, Z. and A. Meijerink, *Ce*(3+)-Doped garnet phosphors: composition modification,
- luminescence properties and applications. Chem Soc Rev, 2017. **46**(1): p. 275-299.
- Bachmann, V., C. Ronda, and A. Meijerink, *Temperature Quenching of Yellow*
- 338 *Ce3+Luminescence in YAG:Ce.* Chemistry of Materials, 2009. **21**(10): p. 2077-2084.
- 339 3. Shao, Q., et al., Temperature-dependent photoluminescence properties of (Y,
- 340 *Lu)3Al5O12:Ce3+ phosphors for white LEDs applications.* Journal of Luminescence, 2011. **341 131**(5): p. 1013-1015.
- Ueda, J., et al., Insight into the Thermal Quenching Mechanism for Y3Al5O12:Ce3+ through
   Thermoluminescence Excitation Spectroscopy. The Journal of Physical Chemistry C, 2015.
   119(44): p. 25003-25008.
- 345 5. Setlur, A.A., et al., Crystal Chemistry and Luminescence of Ce3+-Doped
- 346 Lu2CaMg2(Si,Ge)3O12and Its Use in LED Based Lighting. Chemistry of Materials, 2006. 347 **18**(14): p. 3314-3322.
- Muñoz-García, A.B. and L. Seijo, *Structural, electronic, and spectroscopic effects of Ga*codoping on Ce-doped yttrium aluminum garnet: First-principles study. Physical Review B,
- 350 2010. **82**(18).
- 351 7. Muñoz-García, A.B., et al., Structural effects and 4f-5dtransition shifts induced by La
- codoping in Ce-doped yttrium aluminum garnet: First-principles study. Physical Review B,
   2010. 82(6).
- 354 8. Geller, S., *Crystal chemistry of the garnets*. Zeitschrift für Kristallographie Crystalline Materials, 1967. **125**(1-6): p. 1-47.
- Tauber, A., E. Banks, and H. Kedesdy, *Synthesis of germanate garnets*. Acta Crystallographica, 1958. **11**(12): p. 893-894.
- 358 10. Reinen, D., Die Lichtabsorption des Co2+ und Ni2+ in oxidischen Festk repern mit
- 359 *Granatstruktur. I.* Zeitschrift f**o**r anorganische und allgemeine Chemie, 1964. **327**(3-4): p. 360 238-252.
- Lévy, D. and J. Barbier, Normal and inverse garnets: Ca3Fe2Ge3O12, Ca3Y2Ge3O12and
   Mg3Y2Ge3O12. Acta Crystallographica Section C Crystal Structure Communications, 1999.
   55(10): p. 1611-1614.
- 364 12. Garskaite, E., et al., *Synthesis and Structure of Europium Aluminium Garnet (EAG)*. Zeitschrift für anorganische und allgemeine Chemie, 2007. **633**(7): p. 990-993.
- 366 13. Kasper, H.M., *Series of rare earth garnets Ln3+3M2Li+3O12 (M=Te, W)*. Inorganic Chemistry, 1969. **8**(4): p. 1000-1002.
- Dukhovskaya, E.L., Y.G. Saksonov, and A.G. Titova, *Oxygen parameters of certain compounds of the garnet structure*. Izvestiya Akademii Nauk SSSR, Neorganicheskie Materialy, 1973. **9**(5): p. 809-813.
- Komori, T., et al., Tripraseodymium penta-iron(III) dodeca-oxide, Pr(3)Fe(5)O(12): a
   synchrotron radiation study. Acta Crystallogr Sect E Struct Rep Online, 2009. 65(Pt 11): p.
   i73.
- 16. Komori, T., et al., *Trineodymium(III) penta-iron(III) dodeca-oxide*, *Nd(3)Fe(5)O(12)*. Acta Crystallogr Sect E Struct Rep Online, 2009. **65**(Pt 10): p. i72.
- 376 17. Guo, L., et al., *Mild hydrothermal synthesis and ferrimagnetism of Pr3Fe5O12 and Nd3Fe5O12 garnets.* Journal of Solid State Chemistry, 2011. **184**(5): p. 1048-1053.
- 378 18. Malysa, B., A. Meijerink, and T. Jüstel, *Temperature dependent Cr 3+ photoluminescence in garnets of the type X 3 Sc 2 Ga 3 O 12 (X = Lu, Y, Gd, La)*. Journal of Luminescence, 2018.
- **202**: p. 523-531.
- 381 19. Sawada, H., *Electron Density Study of Garnets:Z3Ga5O12;Z=Nd, Sm, Gd, Tb.* Journal of Solid State Chemistry, 1997. **132**(2): p. 300-307.

- 383 20. Sawada, K., T. Nakamura, and S. Adachi, Europium gallium garnet (Eu3Ga5O12) and
- 384 Eu3GaO6: Synthesis and material properties. Journal of Applied Physics, 2016. **120**(14): p. 143102.
- Awaka, J., et al., *Synthesis and structure analysis of tetragonal Li7La3Zr2O12 with the garnet-related type structure.* Journal of Solid State Chemistry, 2009. **182**(8): p. 2046-2052.
- Murugan, R., et al., *Structure and lithium ion conductivity of garnet-like Li5La3Sb2O12 and Li6SrLa2Sb2O12.* Materials Research Bulletin, 2008. **43**(10): p. 2579-2591.
- Rongjin, J., et al., Glycothermal synthesis of heavily Ce-doped YIG nanocrystals and their microstructures and magnetic properties. Journal of Materials Chemistry C, 2013. 1(9): p. 1763.
- Bugaris, D.E. and H.C. zur Loye, *Materials discovery by flux crystal growth: quaternary and higher order oxides.* Angew Chem Int Ed Engl, 2012. **51**(16): p. 3780-811.
- 395 25. Bruker AXS, I., Madison, Wisconsin, USA, *APEX3 Version 2016.5-0 and SAINT+ Version* 8.37A. 2016.
- 397 26. Krause, L., et al., *Comparison of silver and molybdenum microfocus X-ray sources for single-crystal structure determination.* J Appl Crystallogr, 2015. **48**(Pt 1): p. 3-10.
- 399 27. Sheldrick, G.M., *SHELXT integrated space-group and crystal-structure determination*. Acta Crystallogr A Found Adv, 2015. **71**(Pt 1): p. 3-8.
- 401 28. Hubschle, C.B., G.M. Sheldrick, and B. Dittrich, *ShelXle: a Qt graphical user interface for SHELXL*. J Appl Crystallogr, 2011. **44**(Pt 6): p. 1281-1284.
- 403 29. Izumi, F. and K. Momma, *Three-Dimensional Visualization in Powder Diffraction*. Solid State Phenomena, 2007. **130**: p. 15-20.
- 405 30. Blochl, P.E., *Projector augmented-wave method.* Phys Rev B Condens Matter, 1994. **50**(24): p. 17953-17979.
- 407 31. Kresse, G. and D. Joubert, *From ultrasoft pseudopotentials to the projector augmented-wave method.* Physical Review B, 1999. **59**(3): p. 1758-1775.
- 409 32. Kresse, G. and J. Hafner, *Ab initio molecular dynamics for liquid metals*. Phys Rev B Condens Matter, 1993. **47**(1): p. 558-561.
- 411 33. Kresse, G. and J. Furthmuller, *Efficient iterative schemes for ab initio total-energy*
- 412 *calculations using a plane-wave basis set.* Phys Rev B Condens Matter, 1996. **54**(16): p. 413 11169-11186.
- 414 34. Kresse, G. and J. Furthmüller, *Efficiency of ab-initio total energy calculations for metals and semiconductors using a plane-wave basis set.* Computational Materials Science, 1996. **6**(1):

416 p. 15-50.

- 417 35. Perdew, J.P., et al., *Restoring the density-gradient expansion for exchange in solids and surfaces.* Phys Rev Lett, 2008. **100**(13): p. 136406.
- 419 36. Dudarev, S.L., et al., *PhysRevB.57.1505.pdf>*. Physical Review B, 1998. **57**(3): p. 1505-420 1509.
- Jiang, H., et al., Localized and itinerant states in lanthanide oxides united by GW @ LDA+U.
  Phys Rev Lett, 2009. 102(12): p. 126403.
- 423 38. Jiang, H., P. Rinke, and M. Scheffler, *Electronic properties of lanthanide oxides from theGW perspective*. Physical Review B, 2012. **86**(12).
- Shannon, R.D., *Revised effective ionic radii and systematic studies of interatomic distances in halides and chalcogenides.* Acta Crystallographica Section A, 1976. **32**(5): p. 751-767.
- 427 40. Song, Z., D. Zhou, and Q. Liu, *Tolerance factor and phase stability of the garnet structure*.
- 428 Acta Crystallogr C Struct Chem, 2019. **75**(Pt 10): p. 1353-1358.
- 429 41. Goldschmidt, V.M., *Die Gesetze der Krystallochemie*. Die Naturwissenschaften, 1926.
- 430 **14**(21): p. 477-485.

- 431 42. Jiang, Z., Y. Wang, and L. Wang, Enhanced Yellow-to-Orange Emission of Si-Doped Mg[sub 3]Y[sub 2]Ge[sub 3]O[sub 12]:Ce[sup 3+] Garnet Phosphors for Warm White Light-433 Emitting Diodes. Journal of The Electrochemical Society, 2010. **157**(5): p. J155.
- 43. Wu, J.L., G. Gundiah, and A.K. Cheetham, *Structure–property correlations in Ce-doped*435 *garnet phosphors for use in solid state lighting.* Chemical Physics Letters, 2007. **441**(4-6): p.
  436 250-254.
- 437 44. Seko, A., Y. Koyama, and I. Tanaka, Cluster expansion method for multicomponent systems 438 based on optimal selection of structures for density-functional theory calculations. Physical 439 Review B, 2009. **80**(16).
- 440 45. Blasse, G., W. Schipper, and J.J. Hamelink, *On the quenching of the luminescence of the trivalent cerium ion.* Inorganica Chimica Acta, 1991. **189**(1): p. 77-80.
- 442 46. Pinelli, S., et al., *Study of the visible spectra of Ca3Sc2Ge3O12 garnet crystals doped with Ce3+ or Pr3+*. Optical Materials, 2004. **25**(1): p. 91-99.